AUTHOR(S)
Li, J., Wang, Y., Fan, L., Wang, X., Shang, L., Zhang, H., & Zhao, Y.

TITLE
Liquid metal hybrid antibacterial hydrogel scaffolds from 3D printing for wound healing

YEAR
2024

DOI
10.1016/j.cej.2024.153805

CITATION
Li, J., Wang, Y., Fan, L., Wang, X., Shang, L., Zhang, H., & Zhao, Y. (2024). Liquid metal hybrid antibacterial hydrogel scaffolds from 3D printing for wound healing. *Chemical Engineering Journal*, 496, 153805. https://doi.org/10.1016/j.cej.2024.153805

VERSION
Accepted Manuscript

Liquid metal hybrid antibacterial hydrogel scaffolds from 3D printing for wound healing

Jinbo Li[a, b], Yu Wang[a, c], Lu Fan[a, b], Xiaoju Wang[b], Luoran Shang[a, d, *], Hongbo Zhang[a, b, e, *], Yuanjin Zhao[a, c, *]

[a] Department of Rheumatology and Immunology, Nanjing Drum Tower Hospital, School of Biological Science and Medical Engineering, Southeast University, Nanjing 210096, China

[b] Pharmaceutical Sciences Laboratory, Åbo Akademi University, Turku 20520, Finland

[c] Oujiang Laboratory (Zhejiang Lab for Regenerative Medicine, Vision and Brain Health), Wenzhou Institute, University of Chinese Academy of Sciences, Wenzhou 325001, China

[d] Shanghai Xuhui Central Hospital, Zhongshan-Xuhui Hospital, and the Shanghai Key Laboratory of Medical Epigenetics, the International Co-laboratory of Medical Epigenetics and Metabolism (Ministry of Science and Technology), Institutes of Biomedical Sciences, Fudan University, Shanghai, 200032, China

[e]Turku Bioscience Centre, University of Turku and Åbo Akademi University, Turku, 20520, Finland

E-mail: luoranshang@fudan.edu.cn (L.R.S.); hongbo.zhang@abo.fi (H.B.Z.); yjzhao@seu.edu.cn (Y.J.Z.)

Hydrogels patches hold significant promise for wound healing. Endeavors have been dedicated to the improvement of hydrogel patch functionalities, with the aim of achieving systematic wound management. Herein, we present liquid metal (LM)

hybrid antibacterial hydrogel scaffolds for wound healing *via* the 3D printing strategy. Gelatin/gellan gum-based hydrogel ink is adopted for printing the scaffolds, with LM microdroplets integrated within. Due to the excellent photothermal responsiveness of LM microdroplets, the LM hybrid scaffolds can convert the received near infrared light energy into heat energy, demonstrating controllable antibacterial ability. In addition, vascular endothelial growth factor is introduced into the scaffolds, which can be sustainably released and play an angiogenesis role. *In vivo* animal experiments demonstrate that this hydrogel scaffolds can effectively assit wound closure by eradicating bacterial infection and promoting angiogenesis. Thus, we believe that the proposed LM hybrid hydrogel scaffolds show promising prospects in wound treatment.

Keywords: liquid metal; antibacterial; hydrogel scaffolds; 3D printing; wound healing

Introduction

Wounds are prevalent and severe complications with typical symptoms such as infection, ulcer, and hemorrhage, which affect millions of people worldwide.[1-3] A lot of biomedical patches have been developed for the management of wounds, including adhesives, hydrogels, scaffolds, microneedles, etc.[4-10] Among them, hydrogels show immense potential due to their advantages of tunable compositions and physicochemical properties.[11-13] Notably, various effective bioactive molecules, such as anti-inflammatory agents, antibacterial drugs, or growth factors, can be encapsulated in hydrogels, which accelerate the damage repair and tissue reconstruction processes through drug release.[14-17] Although significant progress has been achieved, there is still room for improvement regarding the design of methodologies for intelligent drug delivery. Of particular interest is the controllability of the antibacterial activity in accordance to the complex would healing process, which is vital for achieving satisfactory therapeutic effects while reducing the risk of

toxicity. As such, novel hydrogel patches with the desired functionalities are still highly anticipated.

In this paper, we proposed multifunctional liquid metal (LM) hybrid hydrogel scaffolds from 3D printing for effective treatment of infected wound, as illustrated in **Figure 1**. LM is a type of metal with a melting point at or near room temperature.[18-20] It possesses favorable flowability while maintaining metallic bonding between atoms like solid metals.[21, 22] Gallium indium eutectic (EGaIn) is widely attractive LMs.[18, 23] They exhibit various intriguing and excellent characteristics such as high thermal/electrical conductivity, biocompatibility, and photothermal responsiveness.[24-28] These advantages make them highly promising in electronics, soft robotics, sensors, and healthcare.[29-35] Notably, the distinctive photothermal responsiveness property is conducive to controllable antibacterial effect, from which novel composite hydrogel patches can be constructed for efficient wound repair. Compared to traditional block hydrogel, the 3D printing strategy enabled better shape flexibility and adaptability, making the scaffold a better solution for wound dressing.[10]

Herein, we developed the desired LM hybrid antibacterial hydrogel scaffolds for wound healing *via* the 3D printing strategy. Under the action of sonication, micro-sized LM droplets were generated in a gelatin solution through ultrasonication. By employing the gelatin and gellan gum, together with LM microdroplets as the hydrogel ink, LM hybrid hydrogel scaffolds were printed. Due to the integration of gelatin and gellan gum, the hydrogel ink showed good temperature sensitive performance and printability. Benefitting from the advantageous photothermal responsiveness of LM, the LM hydrogel scaffolds could effectively convert light energy into heat, which contributed to controllable antibacterial effect. In addition, vascular endothelial growth factor (VEGF) was encapsulated in the hydrogel scaffolds, which was driven to release with the temperature rise of the hydrogel scaffold. Based on these properties, it was demonstrated by *in vivo* animal experiments that the

hydrogel scaffolds effectively accelerated wound closure by eradicating bacterial infection and promoting angiogenesis. These features of the LM hybrid hydrogel scaffolds suggested that they would play an attractive role in wound treatment.

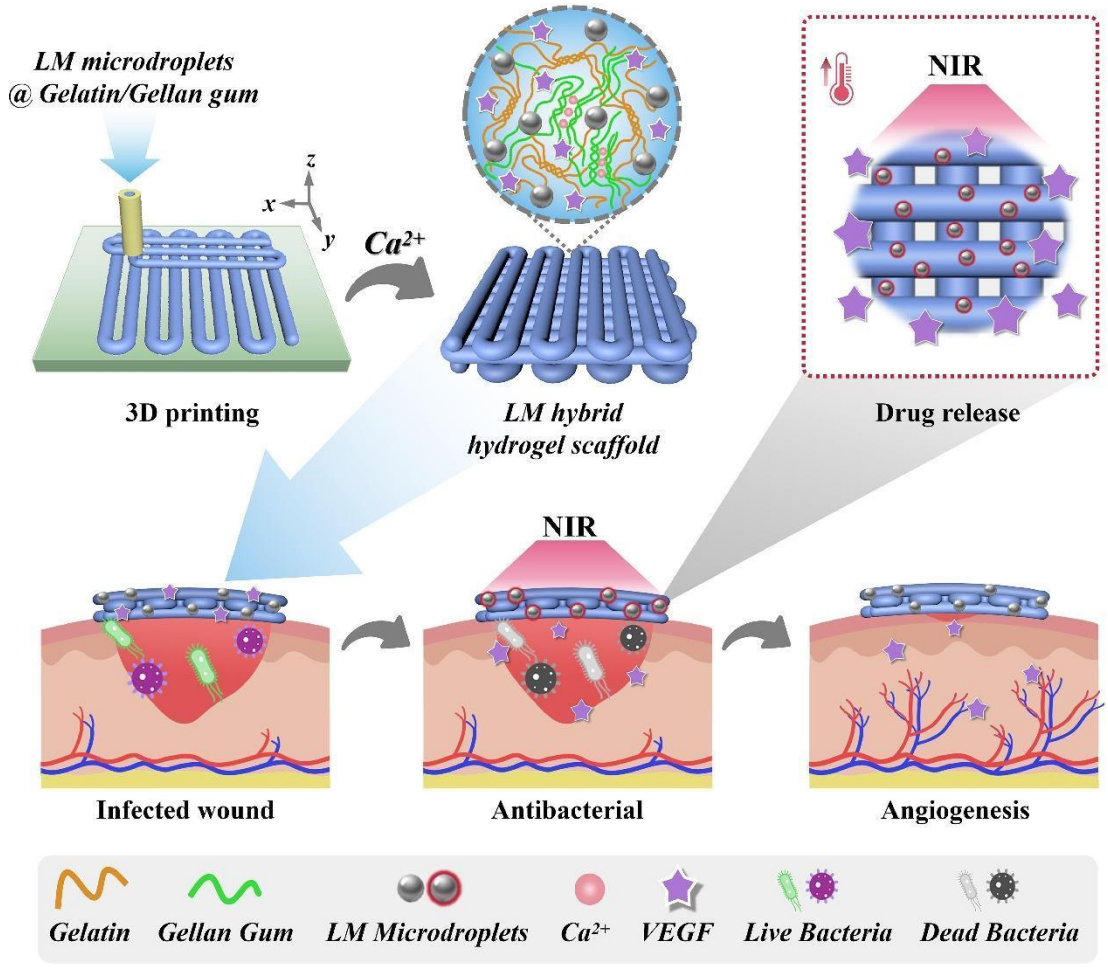

Figure 1 Schematic of the LM hybrid hydrogel scaffold fabrication through the 3D printing technique and its application in treating infected wounds.

Results and Discussion

In a typical experiment, LM microdroplets were prepared by sonication, which mechanically broke a large volume of LM into micro-sized droplets, as shown in **Figure 2a**. The LM microdroplets were produced by sonication of LM bulk in gelatin solution, and subsequently the sonicated LM/gelatin mixture was stored at 4℃ for solidification, thus preventing LM microdroplets from settling. The microstructure of

the LM microdroplets was characterized by a scanning electron microscope (SEM), which showed good sphericity (**Figure 2b**). The particle size statistics showed that the size of the LM microdroplets was 2.199 ± 0.994 μm **(Figure S2a)**. Zeta potential analysis indicated that the LM microdroplets obtained by sonication in DI water and gelatin all carried positive charges (**Figure S2b**).

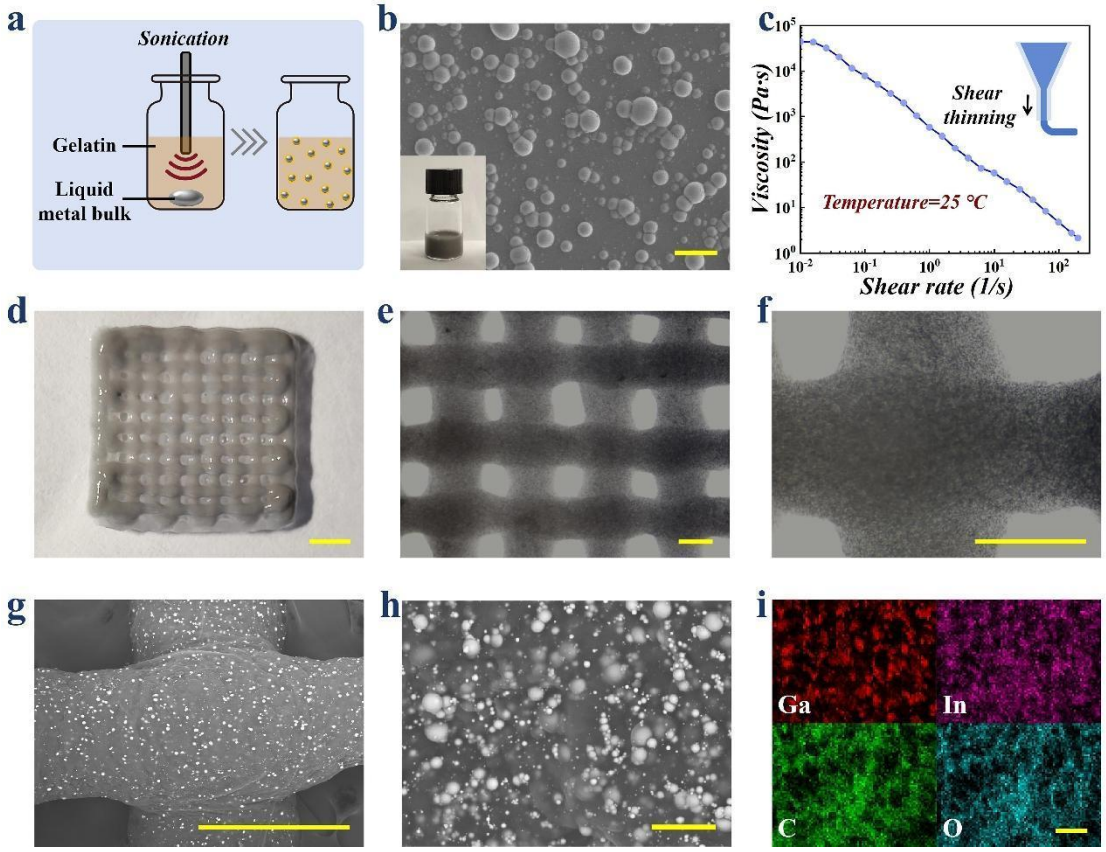

Figure 2 Generation and characterization of the LM hybrid scaffolds. (a) Schematic diagram of the generation of LM microdroplets by ultrasonication in a liquid gelatin solution. (b) SEM images of LM microdroplets. (c) The relationship between viscosity and shear rate of the LM hybrid hydrogel ink. (d) Digital photograph of a printed LM hybrid scaffold. (e) Optical microscopic image of a single-layer LM hybrid scaffold. (f) Optical microscopic image of the intersection of the lateral and vertical paths. (g, h) SEM images of (g) a LM hybrid scaffold and (h) the high-magnification view. (i) EDS analysis results. Scale bars are 10 μm in (b), 2mm in (d), 500 μm in (e-g), and 10 μm in (h, i).

To construct the hybrid scaffolds, the LM/gelatin mixture was mixed with a solution of gellan gum and gelatin to prepare the hydrogel ink for printing (**Figure S1**). The obtained hydrogel ink exhibited gel-to-sol transition at elevated temperatures (**Figure S3**) and showed a typical shear-thinning behavior **(Figure 2c)**. Given this, the ink can be easily extruded from a needle to form a strip-like structure (**Figure S4a**). When the external force was removed, it maintained a complete and clear pattern (**Figure S4b**). With this, LM hybrid scaffolds were printed (**Figure 2d**) with the LM microdroplets embedded in the hydrogel matrix (**Figure 2e, f**). Moreover, to enhance the mechanical strength and stability, the scaffolds were immersed in a calcium chloride ($CaCl_2$) solution to allow the subsequent ionic cross-linking between gellan gum and Ca^{2+}. The morphologies of LM hybrid hydrogels soaked with and without $CaCl_2$ solution before and under NIR irradiation were recorded (**Figure S4c**). The LM hybrid hydrogel soaked in $CaCl_2$ solution remained its original morphology under NIR-induced heating. In contrast, the LM hybrid hydrogel without soaking in $CaCl_2$ melted quickly. The uniform distribution of LM microdroplets in the hydrogel scaffold could be observed from SEM images (**Figure 2g, h**). The high-magnification element distribution of LM hybrid scaffold was also characterized by energy dispersive spectroscopy (EDS) analysis (**Figure 2i**). The uniform distribution of gallium (Ga) and indium (In) in the field of view indicated good dispersion of LM microdroplets. Similarly, in EDS mapping of transverse and vertical intersections, four elements (Ga, In, C, O) also showed the uniform distribution in the LM hybrid scaffold (**Figure S5**). The compression test showed that the modulus of the hydrogel scaffolds increased with more doping of LM microdroplets (**Figure S6**).

Due to the excellent photothermal conversion performance of the embedded LM, the hybrid hydrogel scaffolds would exhibit photothermal. To investigate this, a flower-patterned LM hybrid hydrogel scaffold was constructed, which showed elevated temperatures under NIR irradiation (**Figure S7**). To in-depth explore their photothermal behavior, two parameters involving LM content and NIR energy density were analyzed. It was found that the hybrid hydrogel scaffolds with higher LM

content resulted in faster rise of temperature, and had higher equilibrium temperature (**Figure 3a, Figure S8**). In contrast, the temperature of the scaffolds without LM increased only 4℃ after 5 min. Additionally, the temperature of the LM hybrid hydrogel scaffolds gradually increased with the irradiation time, and their heating rate and equilibrium temperatures could be controlled by the NIR energy density (**Figure 3b**). Typically, the temperature of the hybrid hydrogel scaffolds with 16 mg/mL LM content reached 45℃ after 100 s, and slowly rose to about 50℃. Considering that excessively high temperature will be harmful to normal cells and tissues, the hybrid hydrogel scaffolds with 16 mg/mL LM content under 1 W/cm^2 NIR irradiation was selected for all subsequent photothermal experiments, and the maximum temperature was kept slightly below 50℃. Notably, the LM hybrid hydrogel scaffolds demonstrated cyclic photothermal behavior under periodic NIR irradiation (1 W/cm^2) (**Figure 3c**). Collectively, these results implied that the LM hybrid hydrogel scaffold had controllable and NIR responsiveness, allowing dynamic interactions with the surrounding environment and regulation of local temperature.

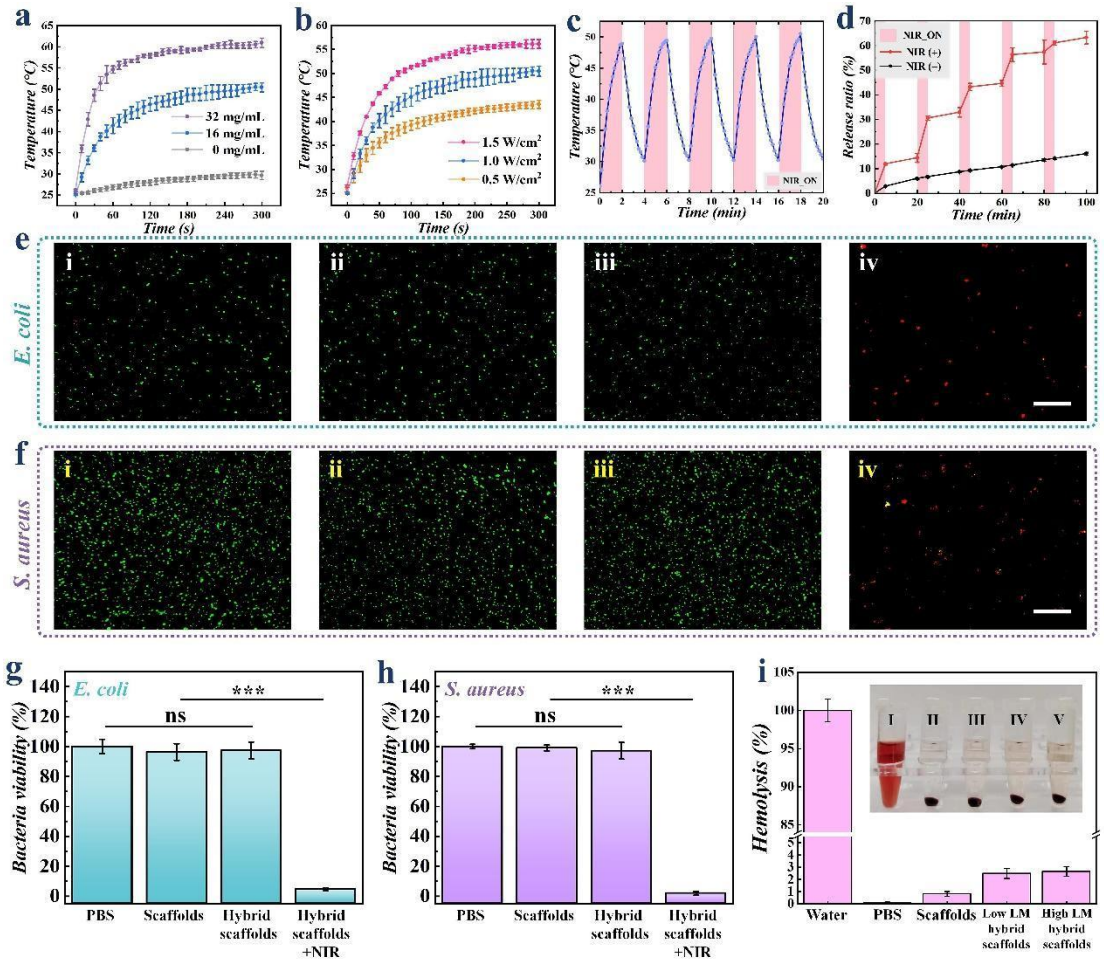

Figure 3 The photothermal properties and antibacterial test of LM hybrid hydrogel scaffolds. (a) Temperature changes of LM hybrid hydrogel scaffolds with different LM concentrations under NIR irradiation (808 nm, 1 W/cm^2). (b) Temperature changes of 16 mg/mL LM hybrid hydrogel scaffolds with NIR irradiation at different intensities (808 nm, 0.5, 1.0, 1.5 W/cm^2). (c) The temperature changes of 16 mg/mL LM hybrid hydrogel scaffolds during 5 laser on/off cycles. (d) The drug release curve of 16 mg/mL LM hybrid hydrogel scaffolds with and without NIR (808 nm, 1 W/cm^2). The red area means that NIR was turned on during that period. (e, f) Live/dead staining of (e) *E. coli* and (f) *S. aureus* treated with (i) PBS, (ii) pure scaffolds without LM, (iii) LM hybrid scaffolds and (iv) LM hybrid scaffolds + NIR. (g, h) Bacterial viability of (g) *E. coli* and (h) *S. aureus* in each group. (i) Hemolysis test. The concentrations of LM in the low LM hybrid scaffolds and high LM hybrid scaffolds were 16 mg/mL and 32 mg/mL respectively. Scale bars are all 200 μm.

VEGF, which has been widely recognized for its role in promoting angiogenesis, was encapsulated in LM hybrid hydrogel scaffolds. We reasoned that the photothermal behavior of the scaffold may have a positive influence on drug release. To simulate the drug release process, fluorescein isothiocyanate labeled bovine serum albumin (FITC-BSA) was applied as a model drug. It was found that LM hybrid hydrogel scaffolds with NIR irradiation exhibited an elevated cumulative amount of drug release compared with that without NIR irradiation (**Figure 3d**). This could be attributed to the enhancement of molecular thermal motion induced by the temperature rise of LM hybrid hydrogel scaffold. Compared with the scaffolds without NIR irradiation, the scaffolds with 5 cycles of NIR irradiation showed weaker fluorescence, indicating a larger amount of release of FITC-BSA (**Figure S9**). Similarly, after each cycle, scaffolds with NIR irradiation released more VEGF than the scaffolds without NIR irradiation (**Figure S10**). The above results demonstrated that controlled drug release could be achieved by applying appropriate NIR irradiation to the LM hybrid hydrogel scaffolds.

The photothermal effect of the LM microdroplets would endow the LM hybrid hydrogel scaffold with antibacterial ability. To investigate this, we evaluated the killing ability of the LM hybrid hydrogel scaffolds against Escherichia coli (*E. coli*) and Staphylococcus aureus (*S. aureus*) respectively. Fluorescent staining images showed that the antibacterial ability of LM hybrid scaffold + NIR group was superior to other groups (**Figure 3e, 3f**). Meanwhile, the quantitative analysis of antibacterial efficacy was conducted (**Figure 3g, 3h**). LM has been applied to wound dressings due to its antibacterial effect under certain conditions. Many of the current studies achieved antibacterial effects by releasing gallium ions.[36] In the present study, the LM hybrid hydrogel scaffolds without NIR irradiation did not exhibit significant antibacterial activity, probably due to the slow release of gallium ions through the hydrogel scaffolds. By contrast, the bacteria death rate of LM hybrid scaffold + NIR group exceeded 95%, proving that the antibacterial effect way mainly induced by photothermal effect. Compared to the control group, the group exposed to NIR

irradiation had faster degradation rates in day 1 and day 2, but both groups exhibited remaining weights above 85% at day 3, which might be attributed to the good stability of the gellan gum (**Figure S11**).

Because of inevitable contact with blood when applied to wounds, the hemocompatibility of LM hybrid hydrogel scaffolds was evaluated based on *in vitro* hemolysis analysis (**Figure 3i**). After different concentrations of LM hybrid hydrogel scaffolds were incubated with RBCs, the measured relative hemolysis rates were all lower than 4%, demonstrating the good blood compatibility of hydrogel scaffolds with/without LM. Besides, the biocompatibility of the LM hybrid hydrogel scaffolds was evaluated by culturing with mouse embryonic fibroblast cells (NIH 3T3 cells) and human umbilical vein endothelial cells (HUVEC cells). For all experimental groups, the corresponding scaffolds were soaked in the cell culture-medium to obtain the leachate for follow-up experiments. To quantitatively evaluate the cell viability, Cell Counting Kit-8 (CCK-8) method was utilized. Results showed that the LM hybrid scaffolds with and without NIR irradiation had the similar cell viabilities as the control group (**Figure 4a, 4b**), and the CCK-8 data further confirmed the biocompatibility of the LM hybrid hydrogel scaffold (**Figure 4d, 4e**). Further, we explored the direct effects of LM hybrid scaffolds under NIR irradiation on HUVEC cells. For the LM hybrid scaffold + NIR group, no large numbers of dead cells were observed in the fluorescence staining images, and the cell viability was above 86% compared to the control group (**Figure S12**).

To examined the proangiogenesis function of the VEGF released from the scaffolds, the human umbilical vein endothelial cells (HUVECs) were utilized for tube formation assay. The corresponding scaffolds were soaked in the cell culture-medium to obtain the leachate for follow-up experiments. More junctions and denser tubes were observed in the VEGF-loaded LM hybrid hydrogel scaffolds (with or without NIR irradiation) groups than in the LM hybrid hydrogel scaffolds (without VEGF) group and control group, as shown in **Figure 4c**. Statistical analysis demonstrated that

the tube lengths of the VEGF-loaded LM hybrid hydrogel scaffolds (with or without NIR irradiation) groups were obviously larger than the other two groups (**Figure 4f**).

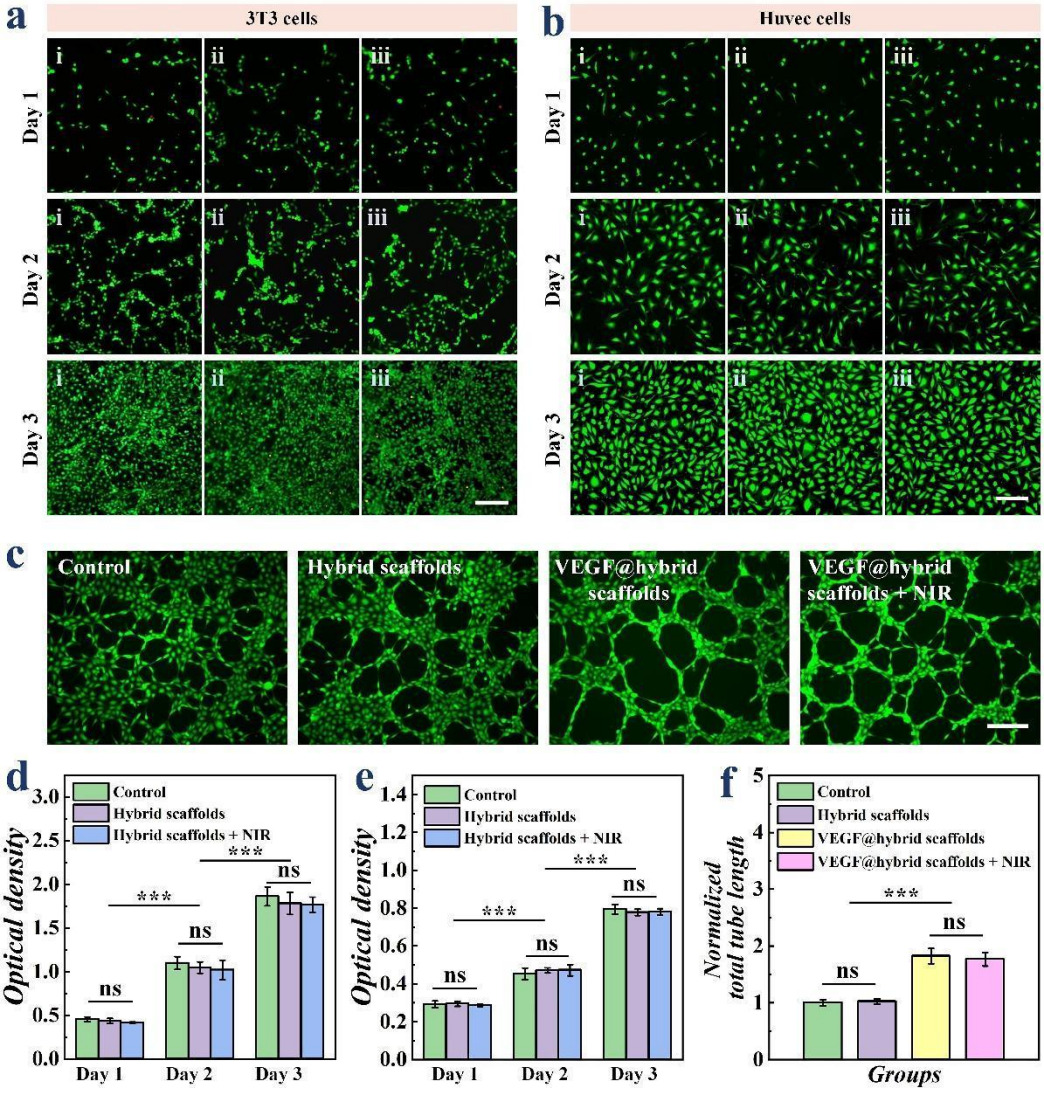

Figure 4 Cytocompatibility and angiogenesis evaluation. (a, b) Fluorescence images of (a) NIH 3T3 cells and (b) HUVEC cells cultured in (i) control group, (ii) LM hybrid hydrogel scaffolds group, and (iii) LM hybrid hydrogel scaffolds with NIR irradiation group during 3 days of culture. (c) Fluorescence images of HUVEC cells cultured in (i) control group, (ii) LM hybrid hydrogel scaffolds group, (iii) VEGF-loaded LM hybrid hydrogel scaffolds group and (iv) VEGF-loaded LM hybrid hydrogel scaffolds with NIR irradiation group. (d, e) Cell viability of NIH 3T3 cells and (e) HUVEC cells cultured in different groups measured by CCK-8. (f) Tube length in different groups. Scale bars are all 200 μm.

Furthermore, to evaluate the potential capability of the LM hybrid hydrogel scaffolds in promoting wound healing, *in vivo* animal experiments were performed. The rats were divided equally into five different groups, including PBS group (control group), LM hybrid hydrogel scaffolds group (Group I), VEGF-loaded LM hybrid hydrogel scaffolds group (Group II), LM hybrid hydrogel scaffolds + NIR group (Group III) and VEGF-loaded LM hybrid hydrogel scaffolds + NIR group (Group IV). The status of the wound sites in different groups were photographed at the corresponding time points, as shown in **Figure 5a**. It was found that the wound area of all groups decreases from day 0 to day 9. Under the action of increased temperature brought by NIR, Group IV showed the fastest closure rate, thanks to the inactivation of bacteria at the wound site and greater VEGF release. In contrast, the wounds in control group and LM hybrid hydrogel scaffolds group (Group I) healed relatively slowly (**Figure 5a, 5b**). The formation of granulation tissue is one of the key stages in the healing of skin wounds. To evaluate the regeneration of granulation tissues, the tissue samples of corresponding groups were treated with hematoxylin-eosin (H&E) staining (**Figure 5d)**. With the increase of collagen in the granulation tissue, the skin wound shrank and the granulation tissue width decreased gradually. Compared to other groups, the Group IV possessed the minimum wound width, as validated in **Figure 5c**. Moreover, the VEGF-loaded LM hybrid hydrogel scaffolds group (Group II) and the LM hybrid hydrogel scaffolds + NIR group (Group III) also showed decreased granulation tissue width. These results indicated that the photothermal antibacterial effect of the scaffolds and the doping of VEGF both had the function of repairing wounds, and could work synergistically.

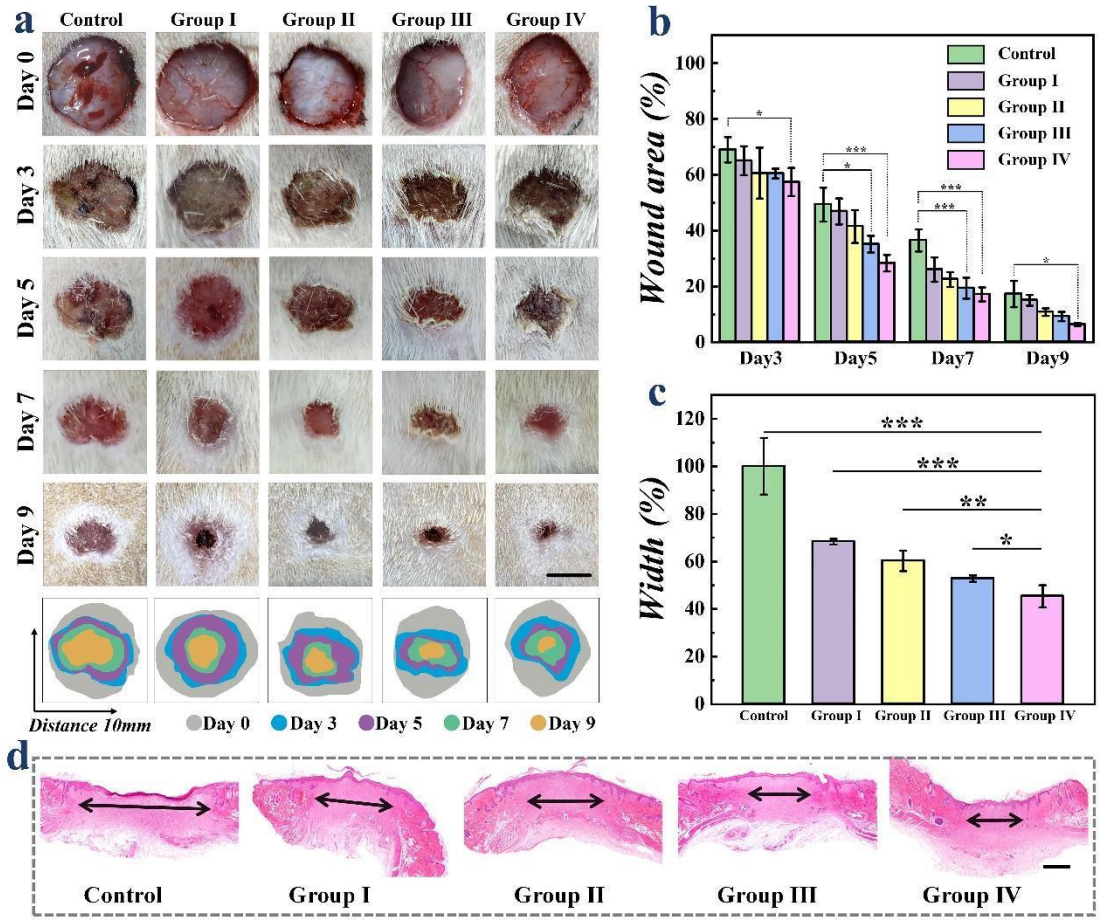

Figure 5 Wound healing application for rats treated with different groups: control group (PBS-treated), Group I (LM hybrid hydrogel scaffolds), Group II (VEGF-loaded LM hybrid hydrogel scaffolds), Group III (LM hybrid hydrogel scaffolds +NIR), and Group IV (VEGF-loaded LM hybrid hydrogel scaffolds +NIR). (a) Representative photographs of the skin wounds. (b) The statistical result of the wound closure situation. (c) Quantitative analysis of the wound width from the HE staining. (d) HE staining of wounds after 9 days, and the double-head arrows represent the width of wounds. Scale bars are 5 mm in (a) and 1 mm in (d).

Inflammation and tissue remodeling are important processes in the wound healing. Accordingly, the levels of inflammatory factors and collagen deposition are important indicators to evaluate the recovery level of the wound site. Immunostaining of Interleukin-6 (IL-6) showed that Group IV had the least level of IL-6 (**Figure 6a, 6d**), which can be attributed to the photothermal antibacterial effect of the hybrid scaffold under NIR. The IL-6 levels in Group II and Group III were also partly suppressed.

Additionally, Masson staining was performed, revealing that Group IV owned the best collagen deposition (**Figure 6b, 6e**), which were consistent with the HE staining results. Moreover, immunostaining of CD31 and α-SMA was applied to reveal the degree of angiogenesis in wound site (**Figure 6c, 6f**). In the control group, a minimal amount of neovascularization was observed. In contrast, the density of neovascularization was significantly higher in Group IV, which confirmed the role of VEGF in accelerating angiogenesis. Thus, benefit from the combined therapy based on NIR and VEGF, Group IV exhibited superiority over the other groups in suppressing infection, depositing collagen, promoting angiogenesis and regenerating tissue.. These outcomes validated the applicability of this LM hybrid scaffold in the field of wound treatment.

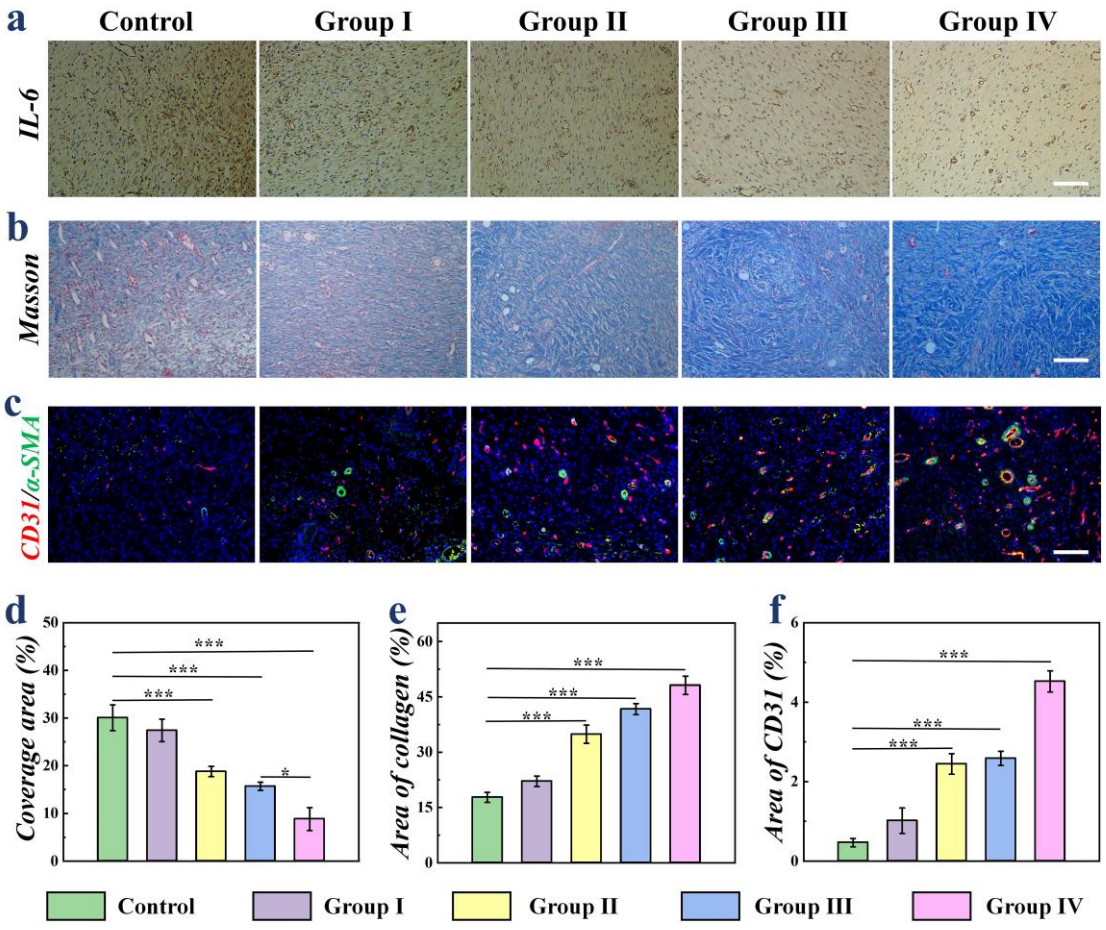

Figure 6 Histological staining analysis of different groups on day 9: control group (PBS-treated), Group I (LM hybrid hydrogel scaffolds), Group II (VEGF-loaded LM hybrid hydrogel scaffolds),

Group III (LM hybrid hydrogel scaffolds +NIR), and Group IV (VEGF-loaded LM hybrid hydrogel scaffolds +NIR). (a) Immunohistochemistry images of IL-6. (b) Masson's trichrome staining images. (c) Double staining of α-SMA and CD31. (d-f) Quantification of the (d) IL-6 area, (e) the collagen deposition area, and (f) the coverage area of CD31. Scale bars are all 100 μm.

Experimental Section

Materials and Reagents

EGaIn was obtained from dingguan metal Co., Ltd. Gelatin and calcium chloride ($CaCl_2$) were all obtained from Sigma-Aldrich (USA). Gellan gum was brought from Macklin (Shanghai, China). FITC-BSA was purchased from Meilunbio (Liaoning, China). PBS buffer solution and VEGF were purchased from Solarbio (Beijing, China). VEGF ELISA Kit was obtained from Elabscience (Wuhan, China). All animal experiments involved in this work were conducted after the permission of Animal Ethics Committee of WIUCA (Wenzhou Institute, University of Chinese Academy of Sciences) (Issue No.: WIUCAS23110203).

Preparation of the LM hybrid hydrogel ink and LM hybrid hydrogel scaffolds

To prepare hydrogel ink with LM microdroplets, we first prepared 10% (w/v) gelatin solution and 3% (w/v) gellan gum solution. Next, the gelatin solution was heated to melt and mixed with LM bulk, and then immediately sonicated (25 kHz, 130 W) them in an ice bath for 3 min (2 s work/4 s stop) to obtain LM/gelatin mixture. Finally, LM/gelatin mixture, 10% gelatin and 3% gellan gum were mixed at 1:1:2 ratio to achieve LM hybrid hydrogel ink. The final concentrations of LM in the ink were 16 mg/mL and 32 mg/mL (as different groups in subsequent experiments). The LM hybrid hydrogel scaffolds were generated by 3D printing method at room temperature using a flat needle (orifice diameter: 200 μm) connected with a syringe. The LM hybrid hydrogel ink extruded from the needle was printed along preset paths. After printing, it was soaked in $CaCl_2$ solution (2% w/v). Finally, the LM hybrid

hydrogel scaffold was obtained after sufficient ion crosslinking reaction of gellan gum and Ca^{2+}.

In *vitro* photothermal antibacterial test

In vitro antibacterial activity of LM hybrid scaffolds against *S. aureus* and *E. coli* was investigated . PBS was used as the control group. Hydrogel scaffolds (1 cm × 1 cm × 2 mm) with 16 mg/mL LM or without LM were first prepared and placed in the 48-well plates. Subsequently, they were sterilized with a UV lamp for more than 1h. The scaffolds (without LM) group, hybrid scaffolds group and hybrid scaffolds + NIR group were co-incubated with 40 μL bacterial solution and 1mL nutrient broth for 6 h, respectively. Among them, the hybrid scaffolds + NIR group received NIR (808 nm, 1 W/cm^2) before adding nutritional broth. The NIR was set to repeat for two cycles and the maximum temperature was kept below 50℃. The antibacterial properties of hybrid scaffolds were tested by the bacterial live/dead staining assay. Briefly, after different treatments, the bacteria cells were co-stained by propidium iodide (PI) for 2 min and SYTO 9 for 20 min in the dark. Subsequently, a fluorescent microscope was utilized to observe and record the bacterial survival states, and then quantification analysis was performed by image processing.

***In vitro* drug release test**

To prepare FITC-BSA-loaded LM hybrid hydrogel scaffolds, FITC-BSA (the final concentration was 1 mg/mL) was mixing with the LM hybrid hydrogel ink (with 16 mg/mL LM). LM hybrid hydrogel scaffolds (1 cm × 1 cm × 2 mm) were placed in 5 mL PBS under 37℃. For NIR(+) group, the LM hybrid hydrogel scaffolds were put under the 808 nm NIR laser and the NIR irradiation was repeated for 5 cycles. For NIR(-) group, the LM hybrid hydrogel scaffolds were not irradiated with NIR. Afterwards, 100 μL of the soaking solution was collected at the designated time points to measure the fluorescence intensity, and subsequently, an equal volume of PBS solution was added**.** Before and after five cycles, different groups of scaffolds

were observed and photographed with a fluorescence microscope. To prepare VEGF-loaded LM hybrid hydrogels, 0.4 mL LM hybrid hydrogel ink was mixed with 100 ng VEGF, and then soaked in 3 mL $CaCl_2$ solution for a cross-linking reaction for 12 h. The hydrogels were then immersed in DI water for the VEGF release experiment, utilizing the VEGF ELISA kit. For NIR(+) group, the NIR laser was modulated to repeat for 5 cycles. Samples were taken for detection at the end of each cycle. For NIR(-) group, the hydrogels were not irradiated with NIR and the samples were taken at the same time points as the NIR(-) group.

***In vitro* degradation test**

Two groups of scaffolds were prepared for degradation testing, with 6 samples per group. For each sample, 0.4 mL LM hybrid hydrogel ink (with 16 mg/mL LM) was completely made into scaffolds by 3D printing, and then soaked in $CaCl_2$ solution for a cross-linking reaction for 12 h. Each scaffold was then washed with DI water and weighed. Subsequently, for NIR(+) group, the NIR was set to repeat for two cycles. For NIR(-) group, the hydrogels was not irradiated with NIR. All scaffolds were individually soaked in PBS solution and weighed every 24 h.

***In vitro* hemolysis analysis**

Fresh rat blood was centrifuged (3000 rpm, 5 min) five times and the supernatant was removed. The obtained clean red blood cells were resuspended in PBS for subsequent use. Water, PBS, scaffolds without LM, and hybrid scaffolds containing low (16 mg/mL) and high (32 mg/mL) LM concentrations were co-incubated with red cell suspension (37℃, 2 h), respectively. Red blood cells (RBCs) co-incubated with water was used as the positive control group (water group), and that co-incubated with PBS was used as the negative control group (PBS group). Thereafter, the mixed solutions were centrifuged, and the supernatant was collected to measure the optical density at 540 nm absorbance.

***In vitro* cytotoxicity test**

The effect of the LM hybrid scaffolds on the growth status of the cells was investigated. LM hybrid scaffolds with and without NIR irradiation were set as the experimental groups, and equal amounts of the LM hybrid scaffolds were immersed in the cell culture-medium for 24 h. For the group of LM hybrid scaffolds with NIR irradiation, the scaffolds were exposed to 2 cycles of NIR irradiation at the beginning of immersion. Then the impurities were filtered out to obtain the leachates. Cell culture-medium was used as the control group. These leachates were separately cocultured with NIH 3T3 cells and HUVEC cells. Moreover, the toxicity of the hybrid hydrogel to the HUVEC cells under the NIR irradiation was also investigated. HUVEC cells were seeded into a 48-well plate at a density of 10^4 cells per well and cultured for 12 hours. The NIR group was exposed to 2 cycles of NIR irradiation, and the hybrid scaffolds + NIR group was exposed to 2 cycles of NIR irradiation after the addition of the LM hybrid scaffolds. Cell morphology and proliferation were visualized using Calcein-AM staining. It was also quantified using CCK-8.

Angiogenesis test

The angiogenesis ability of VEGF-loaded LM hybrid scaffolds was analyzed. 10 μL of matrigel was coated at the bottom of 96-well plates and solidified at 37 °C. 100 μL of HUVEC cells (the density was 2×10^5 cells/mL) were subsequently seeded. The cell culture-medium was set as the control group. LM hybrid hydrogel scaffolds, VEGF-loaded LM hybrid hydrogel scaffolds and VEGF-loaded LM hybrid hydrogel scaffolds with NIR irradiation were used as experimental groups. For the experimental groups, scaffolds were soaked into cell culture-medium for 24 h to obtain the leachate. Among them, for the group of VEGF-loaded LM hybrid hydrogel scaffolds with NIR irradiation, the scaffolds were exposed to 2 cycles of NIR irradiation at the beginning of immersion. Then these leachates were separately cocultured with HUVEC cells. After 10 h of culture, the formation of capillary-like tubes after Calcein-AM staining was taken by fluorescence microscopy.

Wound healing experiments

We constructed full-thickness skin defect rat models with bacterial infection. After anesthesia, the hairs on the back of the SD rats were shaved with an animal razor. Then we constructed 1 cm diameter circular skin wounds with surgical scissors. Subsequently, 200 μL mixture of *E. coli* and *S. aureus* was applied to the surface of the wounds. Briefly, we randomly divided these rats into five groups, including the PBS group (control group), the LM hybrid hydrogel scaffolds group, the VEGF-loaded LM hybrid hydrogel scaffolds group, the LM hybrid hydrogel scaffolds + NIR group, and the VEGF-loaded LM hybrid hydrogel scaffolds + NIR group. For all groups involving NIR irradiation, the NIR was set to repeat for two cycles. The wound status of all rats was recorded on day 0, 3, 5, 7, and 9 using a camera. On day 9, these nascent skin tissues were collected. These tissues were subsequently embedded in paraffin, sectioned, and processed for subsequent staining. H&E staining, immunohistochemical staining for IL-6, Masson trichrome staining, and immunohistochemical staining for CD31 and α-SMA were performed.

Characterization

An optical microscope (Olympus) equipped with a CCD camera was applied for bright-field photography. The microstructure of the LM microdroplets and LM hybrid scaffolds were characterized with SEM (Hitachi, Japan). For zeta potential analysis, The LM bulk was sonicated in DI water and gelatin solution to obtain LM microdroplets at DI water and LM microdroplets at gelatin solution, respectively, and then the LM microdroplets at gelatin solution were washed with DI water for 5 times. The zeta potential of the LM microdroplets were measured by Zetasizer Nano ZS (Malvern, UK). The rheological property of hydrogel ink was tested by a rheometer (DHR-2, TA Instruments, USA) with a temperature control system. The fluorescence density of FITC-BSA was measured using a full-wavelength microplate reader (ThermoFisher, USA). The mechanical property of hydrogel scaffolds was measured by an universal material testing machine (Instron, USA).

Statistical Analysis

Unless otherwise stated, all data was presented as the format of mean ± standard deviation (SD). All statistical sample sizes n≥3. The significant difference analysis involved was calculated through one-way analysis of variance. Specifically, *p < 0.05, **p < 0.01, and ***p < 0.001.

Conclusion

In conclusion, we have developed VEGF-loaded liquid metal hybrid antibacterial hydrogel scaffolds for wound healing from 3D printing. LM microdroplets, together with gelatin and gellan gum, jointly maintained the shape of the hybrid scaffolds. In addition, the ionic crosslinking reaction between gellan gum with Ca^{2+} enhanced the stability of the printed LM hybrid scaffolds. Owing to the excellent photothermal responsiveness of LM microdroplets, the hybrid hydrogel scaffolds were imparted with controllable antibacterial and drug release effects, and could effectively accelerate wound closure by eradicating bacterial infection and promoting angiogenesis. Thus, we believe that the proposed LM hybrid hydrogel scaffolds are expected to provide a new perspective on multifunctional hydrogel dressings in the field of wound healing and other related biomedical applications. Additional cellular gene level analysis can be explored in the future research.

References

[1] M. G. Jeschke, M.E. van Baar, M.A. Choudhry, K.K. Chung, N.S. Gibran, S. Logsetty, Burn injury. Nat. Rev. Dis. Primers 6(1), 11 (2020). https://doi.org/10.1038/s41572-020-0145-5

[2] M. Kharaziha, A. Baidya, N. Annabi, Rational design of immunomodulatory hydrogels for chronic wound healing. Adv. Mater. 33(39), 2100176 (2021). https://doi.org/10.1002/adma.202100176

[3] D.G. Armstrong, A.J. Boulton, S.A. Bus, Diabetic foot ulcers and their recurrence. N. Engl. J. Med. 376(24), 2367-2375 (2017). https://doi.org/10.1056/NEJMra1615439

[4] J. Lan, L. Shi, W. Xiao, X. Zhang, S. Wang, A rapid self-pumping organohydrogel dressing with hydrophilic fractal microchannels to promote burn wound healing. Adv. Mater. 35(38), 2301765 (2023). https://doi.org/10.1002/adma.202301765

[5] G. Theocharidis, H. Yuk, H. Roh, L. Wang, I. Mezghani, J. Wu, A. Kafanas, M. Contreras, B. Sumpio, Z. Li, E. Wang, L. Chen, C.F. Guo, N. Jayaswal, X.L. Katopodi, N. Kalavros, C.S. Nabzdyk, I.S. Vlachos, A. Veves, X. Zhao, A strain-programmed patch for the healing of diabetic wounds. Nat. Biomed. Eng. 6(10), 1118-1133 (2022). https://doi.org/10.1038/s41551-022-00905-2

[6] Y. Wang, Y. Yu, J. Guo, Z. Zhang, X. Zhang, Y. Zhao, Bio-inspired stretchable, adhesive, and conductive structural color film for visually flexible electronics. Adv. Funct. Mater. 30(32), 2000151 (2020). https://doi.org/10.1002/adfm.202000151

[7] X. Cao, L. Sun, D. Xu, S. Miao, N. Li, Y. Zhao, Melanin-integrated structural color hybrid hydrogels for wound healing. Adv. Sci. 10(22) (2023) e2300902. https://doi.org/10.1002/advs.202300902

[8] L. Fan, X. Zhang, M. Nie, Y. Xu, Y. Wang, L. Shang, Y. Zhao, Y. Zhao, Photothermal responsive microspheres-triggered separable microneedles for versatile drug delivery. Adv. Funct. Mater. 32(13), 2110746 (2021). https://doi.org/10.1002/adfm.202110746

[9] W. Li, X. Yang, P. Lai, L. Shang, Bio-inspired adhesive hydrogel for biomedicine-principles and design strategies. Smart Med. 1(1), e20220024 (2022). https://doi.org/10.1002/SMMD.20220024

[10] X. Ding, Y. Yu ,W. Li, Y. Zhao, In situ 3D-bioprinting MoS2 accelerated gelling hydrogel scaffold for promoting chronic diabetic wound healing. Matter 6, 1-15 (2023). https://doi.org/10.1016/j.matt.2023.01.001

[11] D. Seliktar, Designing cell-compatible hydrogels for biomedical applications. Science 336(6085), 1124-1128 (2012). https://doi.org/10.1126/science.1214804

[12] C.O. Chantre, G.M. Gonzalez, S. Ahn, L. Cera, P.H. Campbell, S.P. Hoerstrup, K.K. Parker, Porous biomimetic hyaluronic acid and extracellular matrix protein

nanofiber scaffolds for accelerated cutaneous tissue repair. ACS Appl. Mater. Interfaces 11(49), 45498-45510 (2019). https://doi.org/10.1021/acsami.9b17322

[13] C. Yang, Y. Yu, L. Shang, Y. Zhao, Flexible hemline-shaped microfibers for liquid transport. Nat. Chem. Eng. 1, 87-96 (2024). https://doi.org/10.1038/s44286-023-00001-5

[14] J. Ye, L. Li, R. Hao, M. Gong, T. Wang, J. Song, Q. Meng, N. Zhao, F. Xu, Y. Lvov, L. Zhang, J. Xue, Phase-change composite filled natural nanotubes in hydrogel promote wound healing under photothermally triggered drug release. Bioact. Mater. 21, 284-298 (2023). https://doi.org/10.1016/j.bioactmat.2022.08.026

[15] Y.D.P. Limasale, P. Atallah, C. Werner, U. Freudenberg, R. Zimmermann, Tuning the local availability of VEGF within glycosaminoglycan-based hydrogels to modulate vascular endothelial cell morphogenesis. Adv. Funct. Mater. 30(44), 2000068 (2020). https://doi.org/10.1002/adfm.202000068

[16] J. Guo, Z. Luo, F. Wang, H. Gu, M. Li, Responsive hydrogel microfibers for biomedical engineering. Smart Med. 1(1), e20220003 (2022). https://doi.org/10.1002/SMMD.20220003

[17] Y. Zhi, J. Che, H. Zhu, R. Liu, Y. Zhao, Glycyrrhetinic acid liposomes encapsulated microcapsules from microfluidic electrospray for inflammatory wound healing. Adv. Funct. Mater. 33(43), 2304353 (2023). https://doi.org/10.1002/adfm.202304353

[18] J. Ma, F. Krisnadi, M.H. Vong, M. Kong, O.M. Awartani, M.D. Dickey, Shaping a soft future: patterning liquid metals. Adv. Mater. 35(19), 2205196 (2023). https://doi.org/10.1002/adma.202205196

[19] M. Kim, H. Lim, S.H. Ko, Liquid metal patterning and unique properties for next-generation soft electronics. Adv. Sci. 10(6), 2205795 (2023). https://doi.org/10.1002/advs.202205795

[20] J. Cao, X. Li, Y. Liu, G. Zhu, R.W. Li, Liquid metal-based electronics for on-skin healthcare. Biosensors 13(1), 84 (2023). https://doi.org/10.3390/bios13010084

[21] G. Ryu, K. Park, H. Kim, Interfacial properties of liquid metal immersed in various liquids. J. Colloid Interface Sci. 621, 285-294 (2022). https://doi.org/10.1016/j.jcis.2022.04.037

[22] G. Ryu, I. Park, H. Kim, Liquid metal micro- and nanodroplets: characteristics, fabrication techniques, and applications. ACS Omega 8(18), 15819-15830 (2023). https://doi.org/10.1021/acsomega.3c01382

[23] H. Yu, L. Yu, X. Qi, J. Cui, K. Wu, Y. Liu, L. Chen, X. Li, Versatile chewed gum composites with liquid metal for strain sensing, electromagnetic interference shielding and flexible electronics. J. Mater. Chem. C 11(31), 10455-10463 (2023). https://doi.org/10.1039/d3tc02067c

[24] X. Zhang, G. Chen, L. Sun, F. Ye, X. Shen, Y. Zhao, Claw-inspired microneedle patches with liquid metal encapsulation for accelerating incisional wound healing. Chem. Eng. J. 406, 126741 (2021). https://doi.org/10.1016/j.cej.2020.126741

[25] S. Bi, J. Qi, W, Zhang, X. Jiang, A liquid metal dressing for anti-inflammatory and anti-infection applications to treat diabetic wounds. Chem. Commun. 59(54), 8420-8423 (2023). https://doi.org/10.1039/d3cc01305g

[26] T. Gan, Q. Xiao, S. Handschuh-Wang, X. Huang, H. Wang, X. Deng, S. Hu, B. Wang, Q. Wu, X. Zhou, Conformally adhesive, large-area, solidlike, yet transient liquid metal thin films and patterns via gelatin-regulated droplet deposition and sintering. ACS Appl. Mater. Interfaces 14(37), 42744-42756 (2022). https://doi.org/10.1021/acsami.2c12880

[27] Y. Yu, J. Guo, B. Ma, D. Zhang, Y. Zhao, Liquid metal-integrated ultra-elastic conductive microfibers from microfluidics for wearable electronics. Sci. Bull. 65(20), 1752-1759 (2020). https://doi.org/10.1016/j.scib.2020.06.002

[28] N. Yang, X. Sun, Y Zhou, X. Yang, J. You, Z. Yu, J. Ge, F. Gong, Z. Xiao, Y. Jin, Z. Liu, L. Cheng, Liquid metal microspheres with an eddy-thermal effect for magnetic hyperthermia-enhanced cancer embolization-immunotherapy. Sci. Bull. 68(16), 1772-1783 (2023). https://doi.org/10.1016/j.scib.2020.06.002

[29] Y. Xu, Y. Su, X. Xu, B. Arends, G. Zhao, D. N. Ackerman, H. Huang, S. Reid, J. L. Santarpia, C. Kim, Z. Chen, S. Mahmoud, Y. Ling, A. Brown, Q. Chen, G. Huang, J. Xie, Z. Yan, Porous liquid metal-elastomer composites with high leakage resistance and antimicrobial property for skininterfaced bioelectronics. Sci. Adv. 9(1), eadf0575 (2023). https://doi.org/10.1126/sciadv.adf0575

[30] F. Krisnadi, S. Kim, S. Im, D. Chacko, M.H. Vong, K. Rykaczewski, S. Park, M.D. Dickey, Printable liquid metal foams that grow when watered. Adv. Mater. e2308862 (2024). https://doi.org/10.1002/adma.202308862

[31] B. Chen, Y. Cao, Q. Li, Z. Yan, R. Liu, Y. Zhao, X. Zhang, M. Wu, Y. Qin, C. Sun, W. Yao, Z. Cao, P.M. Ajayan, M.O.L. Chee, P. Dong, Z. Li, J. Shen, M. Ye, Liquid metal-tailored gluten network for protein-based e-skin. Nat. Commun. 13(1), 1206 (2022). https://doi.org/10.1038/s41467-022-28901-9

[32] K. Yamagishi, W. Zhou, T. Ching, S.Y. Huang, M. Hashimoto, Ultra-deformable and tissue-adhesive liquid metal antennas with high wireless powering efficiency. Adv. Mater. 33(26), 2008062 (2021). https://doi.org/10.1002/adma.202008062

[33] Z. Zou, Y. Chen, S. Yuan, N. Luo, J. Li, Y. He, 3D printing of liquid metals: recent advancements and challenges. Adv. Funct. Mater. 33(10), 2213312 (2022). https://doi.org/10.1002/adfm.202213312

[34] R. Xing, J. Yang, D. Zhang, W. Gong, T.V. Neumann, M. Wang, R. Huang, J. Kong, W. Qi, M.D. Dickey, Metallic gels for conductive 3D and 4D printing. Matter 6(7), 2248-2262 (2023). https://doi.org/10.1016/j.matt.2023.06.015

[35] F. Li, J. Shu, L. Zhang, N. Yang, J. Xie, X. Li, L. Cheng, S. Kuang, S.-Y. Tang, S. Zhang, W. Li, L. Sun, D. Sun, Liquid metal droplet robot. Appl. Mater. Today 19, 100597 (2020). https://doi.org/10.1016/j.apmt.2020.100597

[36] D. Negi, Y. Singh, Gallium Oxide Nanoparticle-Loaded, Quaternized Chitosan-Oxidized Sodium Alginate Hydrogels for Treatment of Bacteria-Infected Wounds. ACS Appl. Nano Mater. 6, 13616-13628 (2023). https://doi.org/10.1021/acsanm.3c02266

Acknowledgements

This study is part of the activities of the Åbo Akademi University Foundation (SÅA) funded Center of Excellence in Research "Materials-driven solutions for combating antimicrobial resistance (MADNESS)" at ÅAU. We appreciate the financial support from National Natural Science Foundation of China (82372145); the Research Fellow (Grant No. 353146), Research Project (347897), Solutions for Health Profile (336355), InFLAMES Flagship (337531) grants from Academy of Finland; and the Finland China Food and Health International Pilot Project funded by the Finnish Ministry of Education and Culture.

Author contributions

Y.J.Z. and L.R.S. conceived the idea and designed the experiment. J.B.L. conducted experiments and data analysis. J.B.L., Y.W. and Lu Fan wrote the manuscript. X.J. W., H.B.Z. and L.R.S. assisted with paper writing.

Additional information

Supplementary Information accompanies this paper is available.

Competing financial interests: The authors declare no competing financial interests.